한국지반공학회논문집 제20권 5호 2004년 7월 pp. 5 ~ 16 / 특별논문집 제1호 /

# A Study on the Confining Effect Due to Geosynthetics Wrapping Compacted Soil Specimen

## 토목섬유로 보강된 다짐토 공시체의 구속효과에 관한 연구

Kim, Eun-Ra[1] 김 은 라 Iizuka, Atsushi[2]

Kim, You-Seong[3] 김 유 성 Park, Hong[4] 박 홍

### 요 지

본 연구에서는 토목섬유로 보강된 다짐토의 보강 메카니즘이 제시되며, 이러한 보강 메카니즘은 다짐토의 체적팽창(부의 다일러탄시)을 토목섬유에 의해 구속 억제하는 과정에서 생성되는 효과로 간주된다. 먼저, 실내실험을 위한 구체적인 방법으로서, 토목섬유의 보강효과를 정량적으로 파악하기 위하여 사질토를 다짐하여 공시체를 만들어 그 주위에 토목섬유를 설치한 후 전체적으로 압축전단시험을 실시하였다. 실험에서 초기 다짐도는 각각의 종류에 대하여 다일러탄시의 특성이 다르기 때문에 각각의 공시체에 대하여 변화시켰다. 여기서 전단시험 도중에 다짐토의 다일러탄시 변형을 방지하기 위한 토목섬유에 작용하는 축방향 힘들(axial forces)이 조사되었다. 또한 다짐토의 탄소성 모델과 이러한 모델에 필요한 초기 입력치 값의 결정 방법들이 제시된다. 마지막으로, 탄소성 구성 모델에서 항복 이전의 탄성영역의 거동을 모사하기 위하여 Hashiguch(1989)가 제안한 subloading surface의 개념을 도입하여, 유한요소(FEM) 해석을 통해 얻어진 결과들을 실내시험의 결과와 비교 분석하였다.

### Abstract

This paper presents the modeling of geosynthetic-reinforced compacted soils and discusses the reinforcement effect arising from confining the dilatancy deformation of the soil by geosynthetics. A series of compressive shear tests for compacted sandy soil specimens wrapped by geosynthetics are carried out by quantitatively examining the geosynthetic-reinforcement effect, occurring from a confinement of the dilative deformation in compacted soils during shearing. In the test, the initial degree of compaction is changed for each series of sandy soil specimens so that each series has different degree of dilatancy characteristics. Herein, the axial forces working on the geosynthetics so as to prevent dilative deformation of compacted soils during shearing are measured. Furthermore, the elasto-plastic modeling of compacted soils and a rational determination procedure for input parameters needed in the elasto-plastic modeling are presented. And to describe the irreversible deformation characteristics of compacted soils during shearing, the subloading yielding surface (Hashiguchi (1989)) to the elasto-plastic modeling is introduced. Finally, the elasto-plastic finite element simulation is carried out and the geosynthetic-reinforcement effect is discussed.

**Keywords** : Compacted soils, Elasto-plastic modeling, Geosynthetic-reinforcement

1 Member, Dept. of Civil Engrg., Research Center of Industrial Technology, Chonbuk National Univ. (kimeunra@chonbuk.ac.kr)
2 Associate Prof., Dept. of Architecture and Civil Engrg., Kobe Univ.
3 Member, Associate Prof., Dept. of Civil Engrg., Research Center of Industrial Technology, Chonbuk National Univ.
4 Member, Dept. of Geotechnical Engrg., LG Engrg. & Construction Co. Ltd.

## 1. Introduction

The geosynthetic-reinforced soil structures consist of two elements: one is compacted soil and the other is geosynthetics. The reinforcing effect should not be interpreted as that the strength and rigidity of soil itself are merely supplemented by geosynthetic-reinforcement but be understood as that soils and the geosynthetics are unified, and show their fresh strength and rigidity as a composite material. The strength and rigidity of geosynthetic-reinforced soil structure do not come out as the mere summation of strengths and rigidities of soils and geosynthetics. They appear as a result of mechanical interaction between soils and geosynthetics. Many reviews (McGown et al.1978; Jewell 1991) have attempted to clarify the confining effect in reinforcement, and among them the results of Jewell (1991) have generally been used for all stages from laboratory test to its design.

In this research, upon analyzing experimental results in order to clarify the confining effect in geosynthetics, the relation between compaction degree in the soil and confining effect in the geosynthetics was examined in detail. Since the reinforcing effect in geosynthetics is one of confining the dilatancy response in compacted soil, a model test under compressive and shear on a specimen wrapped by geosynthetics is carried out to evaluate the confining effect remarkably. Herein, the soil which compacted is modeled by the Sekiguchi and Ohta's elasto-plastic constitutive model, in which the subloading surface proposed by Hashiguchi (1989) is applied. Therefore, with this new model, the authors could express the dilatancy characteristics, when the current stress state is located inside the yielding surface.

## 2. Experiments

### 2.1 The Used Soil and Preparatory Laboratory Tests

The soil used in experiment is the Pleistocene sand named Omma sand, sampled from Taiyogaoka, Kanazawa, Japan. The specific gravity of soil particle is 2.740, the grain size distribution is the gravel fraction (2 to 75mm) of 2%, the sand fraction (75mm to 2mm) of 80%, the silt fraction (5mm to 75mm) of 11% and the clay fraction (less than 5mm) of 7 %, respectively. The uniformity coefficient is 21.8 and the maximum grain size is 9.5mm. In the preparatory laboratory tests, two kinds of soil specimens were prepared: one is completely disturbed (loosened) sample of which water contents were adjusted to prescribed values (25%) as straddling the optimum water content of 18.8%, and the other was undisturbed (compacted) sample which were compacted aiming at the optimum water content of 18.8%.

A series of shear box tests (SBT) were carried out. Both disturbed and undisturbed samples were subjected to shear under the condition of constant volume after completing Ko-consolidation with vertical pressure of 39.2, 78.4, 156.8 and 313kPa. Test results are summarized in Fig. 1 for disturbed (very loosed) sample and in Fig. 2

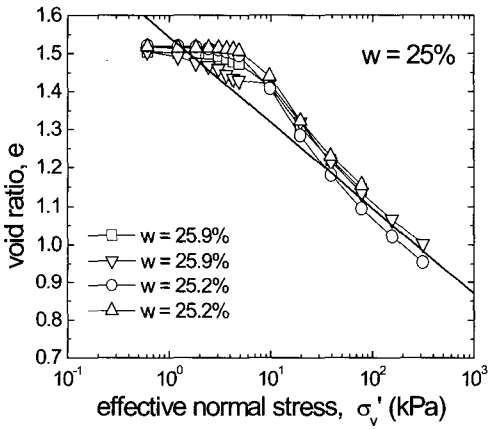


(a) Compression lines of disturbed (very loosed) soil specimens

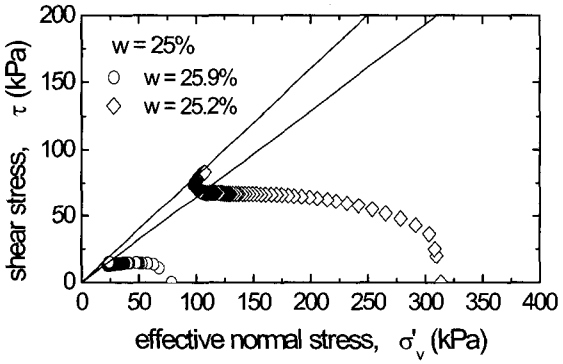


(b) Shear properties of disturbed (very loosed) soil specimens

Fig. 1. Mechanical properties of disturbed sample(very loosed) from SBT

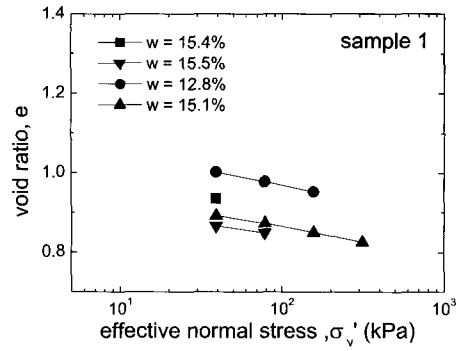


(a) Compression lines of undisturbed (compacted) soil specimens

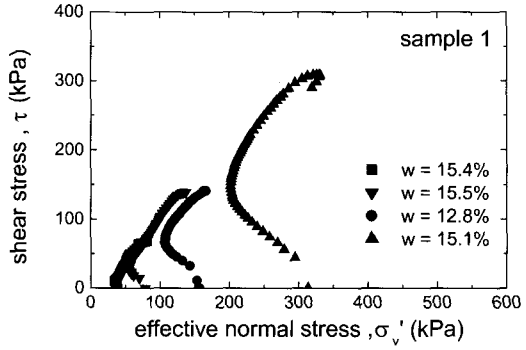


(b) Shear properties of undisturbed (compacted) soil specimens

Fig. 2. Mechanical properties of undisturbed (compacted) sample from SBT

for undisturbed (compacted) sample. Upper figures indicate the compression curves in Ko-consolidation and lower ones the effective stress paths in shear process under the condition of constant volume. By comparing Figs. 1 and 2, the similarity with saturated clays in both compressibility and dilatancy characteristics can be recognized. Namely, the disturbed (compacted) sample behaves like the overconsolidated clay in contrast with the behavior of disturbed (loosed) sample in normally consolidated clay.

## 2.2 Compressive Shear Test

The Omma sand with the prescribed water was uniformly compacted by rammer of 3.5kg up to a designated degree of compaction, and it was wrapped by geosynthetics as shown in Fig. 3. The soil was spread in the thickness of 40 to 80mm for each compaction. The compacted soil specimen (30cm in diameter and 40cm in height) was laid on the uniaxial loading apparatus as

Table 1. Prepared compacted soil specimens for test

| test No | degree of compaction (the number of compaction)×(layers) | water content w(%) | dry density $\rho_d(g/cm^3)$ |
|---|---|---|---|
| 2 | 50×10 | 18.1 | 1.53 |
| 3 | 50×10 | 17.6 | 1.56 |
| 4 | 50×10 | 17.3 | 1.60 |
| 5 | 50×10 | 17.1 | 1.54 |
| 6 | 30×6 | 16.6 | 1.43 |
| 7 | 30×6 | 17.0 | 1.43 |
| 8 | 25×5 | 16.8 | 1.45 |
| 9 | 50×10 | 16.5 | 1.55 |

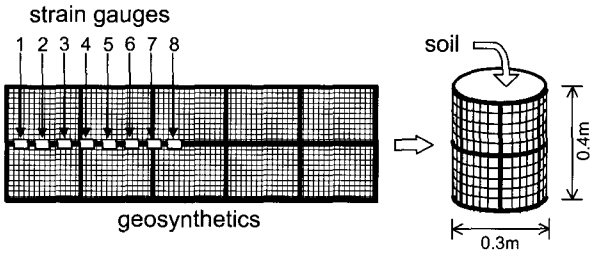


Fig. 3. Strain gauges are installed on geosynthetics to measure extension force

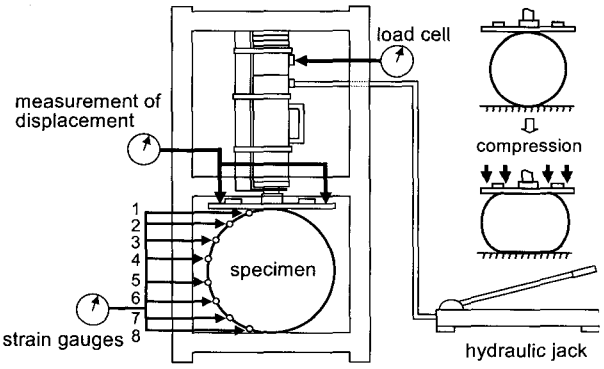


Fig. 4. A schematic of compressive shear apparatus

shown in Fig. 4 and was subjected to compressive shear (Iizuka et al., 2002). Table 1 summarizes the prepared compacted soil specimens for the test. Here, the number of compaction and the spread thickness were varied with the specimen. Some specimens with lower degree of compaction (tests 6 to 8 in Table 1) were also prepared to investigate the influence on the geosynthetic-reinforcement effect due to the difference of the dilatancy characteristics of compacted soil. Herein, in order to measure the extension forces working on geosynthetics, strain gauges are tightly pasted on the geosynthetics as shown in Fig. 3. In the experiment, the vertical dis-

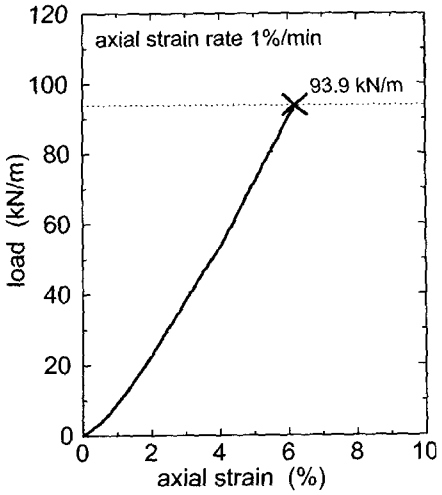


Fig. 5. Stress-strain relation of geosynthetics obtained from uniaxial extension test

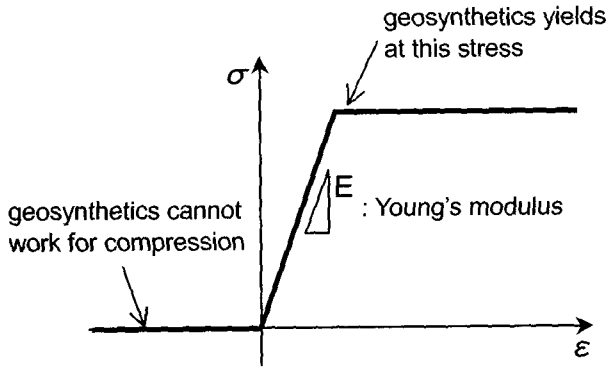


Fig. 6. Geosynthetics model (bar element)

placement of the specimen and the extension stress working on the geosynthetics were measured by using the applied vertical load, as shown in Fig. 4. The compressive shear test was carried out at sufficiently slow rate in order to satisfy the condition that the volume of specimen should be changeable (drained condition).

In the geosynthetic materials used in the experiment, the uniaxial extension test was carried out to measure the stiffness and the ultimate strength of the geosynthetics. Figure 5 shows the stress-strain relation of geosynthetics obtained from the uniaxial extension test. Then, the extension strength is 93.9kN/m, the cross sectional area is $3.2\times10^{-4}m^2$ and Young's modulus is $4.86\times10^{6}kPa$, respectively. Therefore, the geosynthetics have to be modeled as a linearly elastic material as shown in Fig. 6. Photo 2 indicates a snapshot during the test.

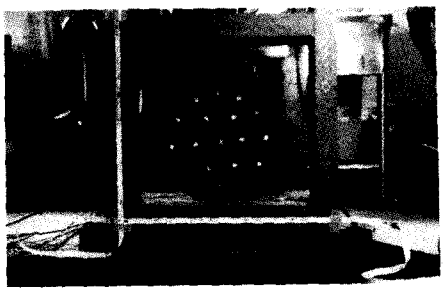

(a) Initial figure of test

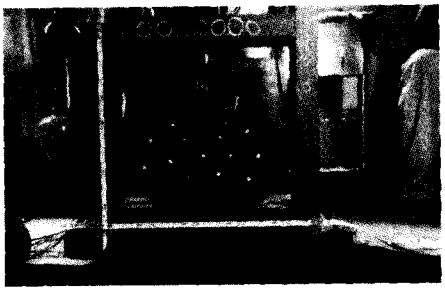

(b) Compressive displacement of 80 mm (test 6)

Photo 1. View of compressive shear test

## 2.3 Results of Compressive Shear Test

The load and displacement relations obtained from the compressive shear model test are shown in Fig. 7. It is found that the well-compacted soil specimens (higher degree of compaction) indicated by the filled symbols (■, ●, ▲, ▼ and ◆) show higher rigidity than the lower-compacted soil specimens by hollow symbols (□, ○ and △). Figure 8 shows extension forces working on the geosynthetics at locations of No.2 and No.4 (see, Fig. 4). As the initial degree of compaction is, higher the extension force gets higher with the displacement. The

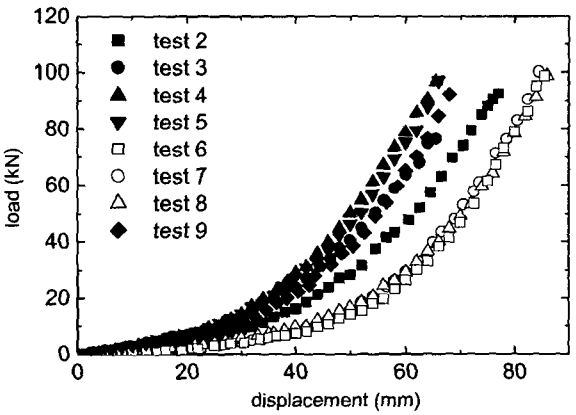


Fig. 7. Load and displacement relation

confining effect in the deformation of soil specimen by geosynthetics can be more obviously recognized when the initial compaction degree of the specimen is higher. Namely, the geosynthetics works more remarkably so as to prevent the dilative deformation of soil specimen, when the soil specimen has higher degree of compaction. Therefore, the reinforcement effect by geosynthetics has close relation with the dilatancy characteristics of soils, since well-compacted soil specimens (higher degree of compaction) tend to more dilate during shear.

Figure 9 shows the distribution of extension force working on the geosynthetics along the circumference of the specimens, when the compressive displacement reaches respectively 10, 20, ··· 80mm. It can be seen that the distribution of extension force along the circumference of specimen is almost uniform regardless of its location. Herein, note that the case of well-compacted specimens is represented by test 5, the case of relatively loose specimens is by test 6, respectively. Here, $\theta$=0 denotes the location at the top of specimen.

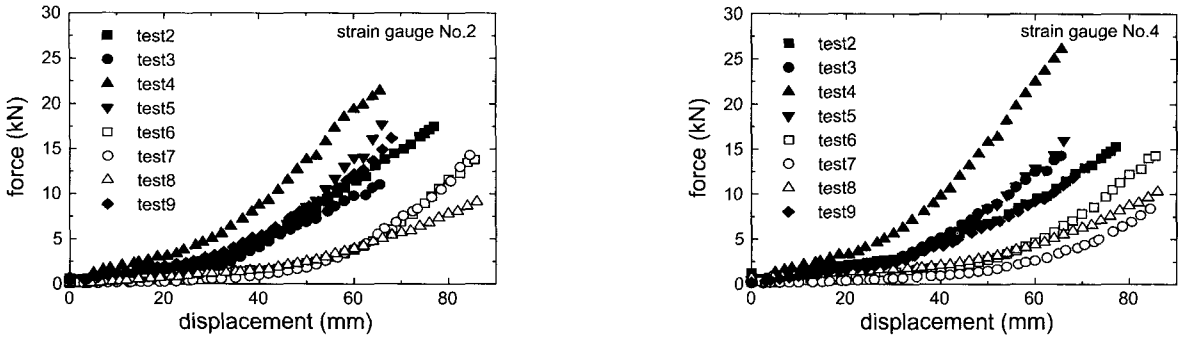


(a) At strain gauge No.2 (b) At strain gauge No.4

Fig. 8. Development of axial forces working to geosynthetics with displacement

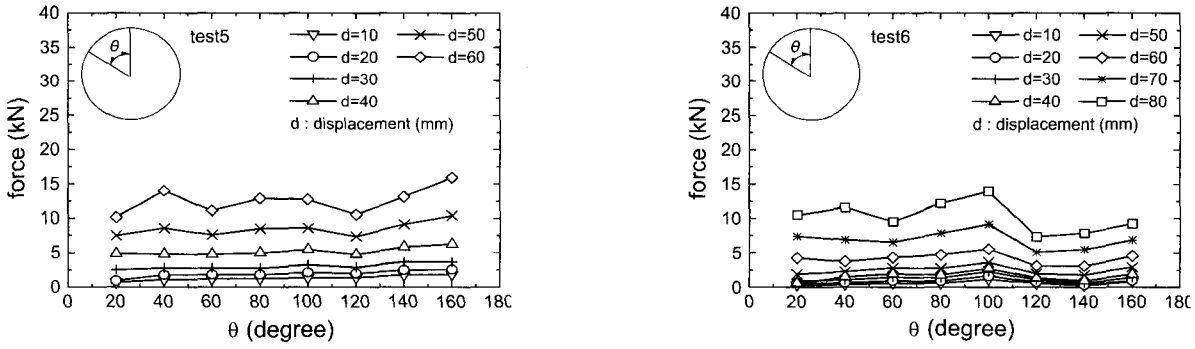


(a) Well compacted specimen (b) Relatively poorly compacted specimen

Fig. 9. Extension forces working to geosynthetics along circumference of specimen

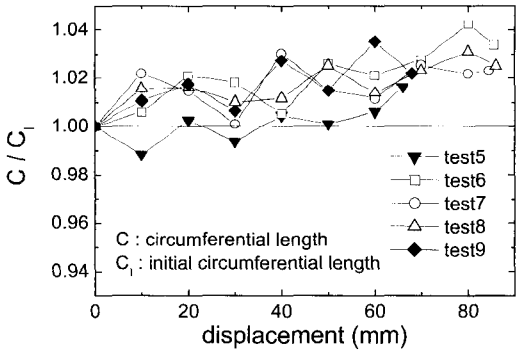


Fig. 10. Change of circumference length

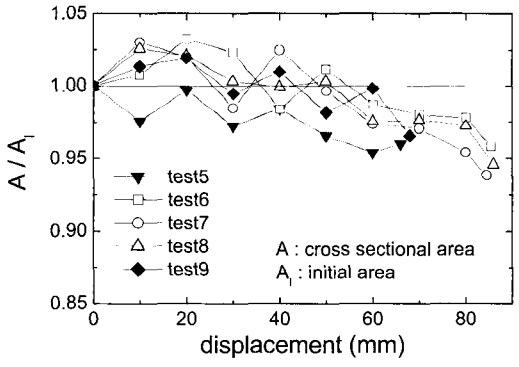


Fig. 11. Change of cross sectional area

The changes of circumference length and cross sectional area during compression are indicated in Figs. 10 and 11. The circumference length of specimen gradually increases regardless of the initial compaction degree. The cross sectional area of specimen, on the contrary, decreases regardless of the initial compaction degree in all the tests.

## 3. Comparison of Measured and Analyzed Result

### 3.1 Condition of Analysis and Preliminary Elastic Simulation

A series of finite element simulation of the compressive shear model tests were carried out. Figure 12 shows the finite element modeling of the test, where quadrilateral constant strain element with 4 nodes is employed. To simulate the compressive shear tests, the displacement is vertically installed to the specimen at the strain rate of 1.0 %/min as indicated in Fig. 12.

To begin with, as a preliminary simulation, the compacted soil is regarded as a linearly elastic material that has no irreversible dilatancy characteristics associated with shearing. And also, based on the uniaxial extension test result of geosynthetics (Fig. 5), the geosynthetics wrapping the soil specimen is modeled by linear elastic bar elements as shown in Fig. 6. The properties are the Young's modulus of $E=4.86\times10^{6}$kPa, the cross sectional area of $A=3.2\times10^{-4}m^2$ and the compression strength of $N_f$=93.9 kN/m, respectively. In the computation, it is assumed that the bar elements (modeling the geosynthetics) do not resist against the axial compression as indicated in Fig. 6.

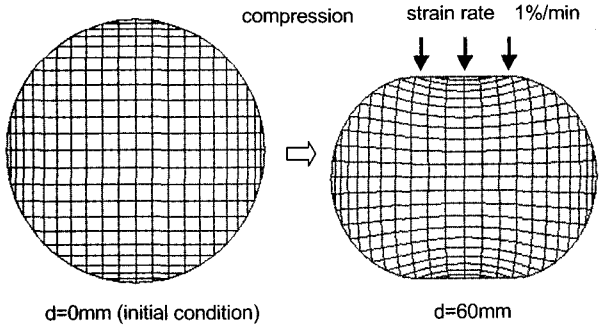


Fig. 12. A schematic of finite element mesh employment

Figure 13 compares the load and displacement relation obtained from the experiments with the computed ones. Here, three values of the Young's modulus for the compacted soil are chosen as shown in the figure, but Poisson's ratio is uniquely assumed to be 0.33 in all cases. The case of E=6000kPa seems to effectively explain the load and displacement relation of well-compacted specimen, test 5 (see, Table 1). Changes in the cross-sectional area and the circumferential length of the specimen are compared in Figs. 14 and 15, respectively. A Young's modulus of 6000kPa is used in the computation, while Poisson's ratio is varied from 0.2 to 0.499 in each case. As for the cross-sectional area of the specimen in Fig. 14, all the cases seem to be able to

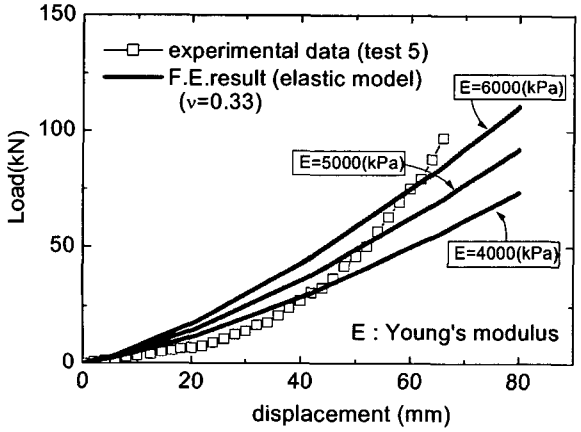


Fig. 13. Computed load and displacement relation with experimental result

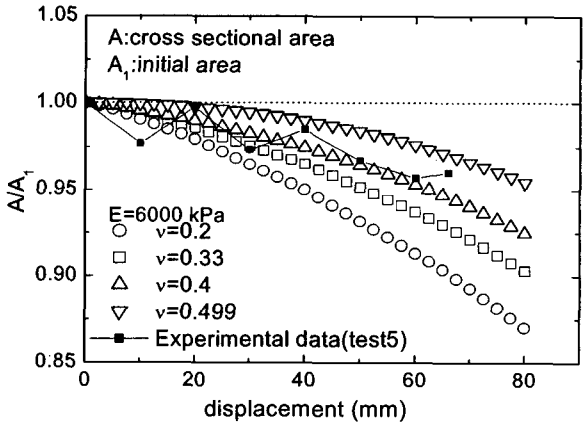


Fig. 14. Computed cross sectional area for various Poisson ratio(elastic model)

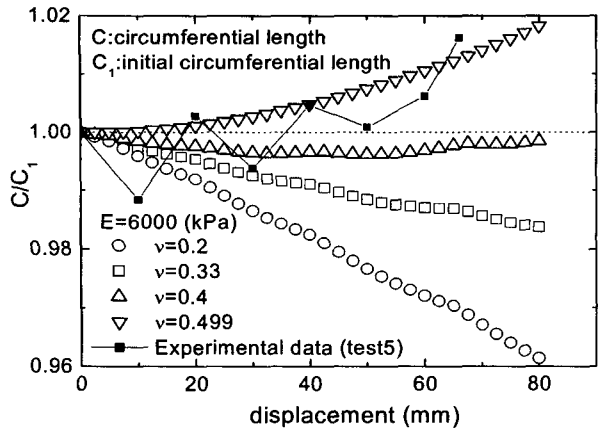


Fig. 15. Computed circumference length for various Poisson ratio (elastic model)

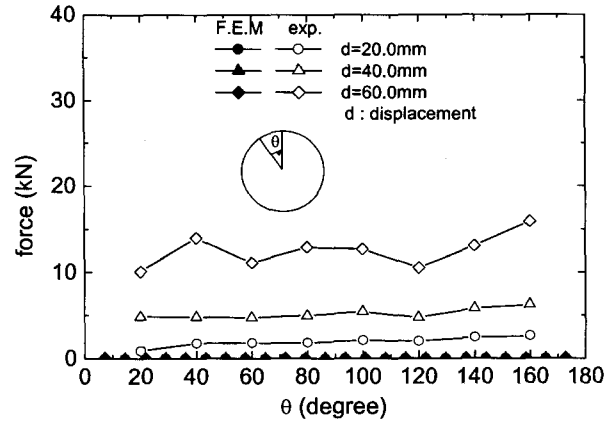


Fig. 16. Extension forces along circumference of specimen (elastic model) (E=6000 kPa and $\nu$=0.33 for test5)

describe the tendency that the experiments show (the cross sectional area decreases with loading). However, as for the circumferential length of the specimen as shown in Fig. 15, only the case of $\nu$=0.499 can explain the experimental results of test 5. The assumption of $\nu$ =0.499 theoretically means an almost incompressible condition and is not acceptable as Poisson's ratio of the soil materials in engineering practice. Figure16 compares the computed distribution of extension forces working to the geosynthetics with the measured ones in test 5. It can be concluded that the elastic assumption, which does not consider the dilatancy characteristics during compressive shearing for the compacted soil, cannot explain the geosynthetic-reinforcement effect observed in the model tests.

## 3.2 Elasto-plastic Finite Element Simulation

### 3.2.1 Elasto-Plastic Modeling of Compacted Soil

In this research, therefore, a conventional elasto-plastic constitutive model, proposed by Sekiguchi and Ohta (1977), should be employed and the subloading surface concept originally proposed by Hashiguchi (1989) is introduced to secure the description ability inside the normal yielding surface, as Fig. 17. Here, the constitutive model by Sekiguchi and Ohta (1977) can be regarded as an extension of the original Cam clay model, but it is distinguished from the Cam-clay model on description ability of the mechanical behavior, which arose from initial anisotropy and stress reorientation. The determination procedure of input parameters needed in the constitutive model has been well established through a lot of practical case studies using a finite element code, DACSAR, which is employed in the Sekiguchi and Ohta's model (Iizuka and Ohta, 1987; Mestat, 2001).

### Sekiguchi and Ohta'S Model with Subloading Surface

The normal yielding function of the Sekiguchi and Ohta's model is expressed as,

$$f=\frac{\lambda-k}{1+e_0}\ln\frac{p'}{p_0'}+D\eta^*-\varepsilon_v^p=0 \qquad (1)$$

where $D$ is the coefficient of dilatancy (Shibata, 1968), $\varepsilon_v^p$ is the volumetric strain, $\lambda(=0.434C_c)$ and $k(=0.434C_s)$

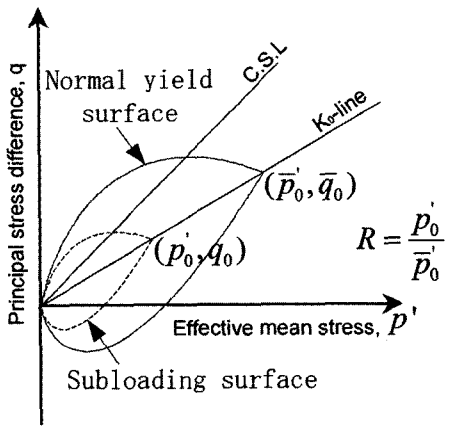


Fig. 17. Illustration of subloading surface concept

are the compression and swelling indices, respectively. The parameters of $\lambda$, $k$ and $D$ have a theoretical relation with the critical state parameter, $M$, as $M=\frac{\lambda-k}{D(1+e_0)}$ (Ohta, 1971). $\eta^*$ is the generalized deviatoric stress parameter, which defined as

$$\eta^*=\sqrt{\frac{3}{2}}\left\| \frac{\mathbf{s}}{p'}-\frac{\mathbf{s}_0}{p'_0} \right\| \quad (2)$$

where $\mathbf{s}$ is the deviatoric stress tensor, the subscript 0 denotes the value at the reference and $\|\cdot\|$ is the Euclid norm. After Hashiguchi (1989), the subloading surface $f_s$ similar to the normal yielding surface can be defined using the similarity ratio $R$, as,

$$f_s=\frac{\lambda-k}{1+e_0}\ln\frac{p'}{p'_0}+D\eta^*-(\varepsilon_v^p+\frac{\lambda-k}{1+e_0}\ln R)=0 \quad (3)$$

where the similarity ratio $R$ determines the scale of subloading yielding surface against the normal yielding surface and is defined as $p'/\overline{p'}$ using the current effective mean stress, $p'$ on the subloading yielding surface and its conjugate effective mean stress, $\overline{p'}$ on the normal yielding surface. The evaluation law of the similarity ratio, $\dot{R}$ is assumed as,

$$\dot{R}=U_R\|\dot{\boldsymbol{\varepsilon}}^p\|=-\frac{m}{D}(\ln R)\|\dot{\boldsymbol{\varepsilon}}^p\| \quad \text{for} \quad \dot{\boldsymbol{\varepsilon}}^p\neq\mathbf{0} \quad (4)$$

the parameter $m$ is the newly introduced material parameter controlling the accessibility rate of the subloading surface to the normal yielding surface. Herein, note that the scalar function, $U_R$ is defined in the region of $0<R\leq1$ and satisfies $U_R=\infty$ at $R$=0 and $U_R=0$ at $R$=1.

Since the current effective stress always stays on the subloading surface, the consistency condition can be described as $\dot{f}_s=0$. Therefore, assuming the associated flow rule as $\dot{\boldsymbol{\varepsilon}}^p=\Lambda\frac{\partial f_s}{\partial\boldsymbol{\sigma}'}$ and introducing the genera lized Hooke's law for describing the elastic region as $\dot{\boldsymbol{\sigma}}'=\boldsymbol{D}^e\dot{\boldsymbol{\varepsilon}}^e=\boldsymbol{D}^e(\dot{\boldsymbol{\varepsilon}}-\dot{\boldsymbol{\varepsilon}}^p)$, the plasticity multiplier of $\Lambda$ is determined as,

$$\Lambda=\frac{1}{h}\frac{\partial f_s}{\partial\boldsymbol{\sigma}}\cdot\dot{\boldsymbol{\sigma}}=\frac{1}{H}\frac{\partial f_s}{\partial\boldsymbol{\sigma}}\cdot\boldsymbol{D}^e\dot{\boldsymbol{\varepsilon}} \quad (5)$$

$$h=tr\left(\frac{\partial f_s}{\partial\boldsymbol{\sigma}}\right)-mM\frac{\ln R}{R}\left\|\frac{\partial f}{\partial\boldsymbol{s}}\right\|, \text{ and}$$

$$H=h+\frac{\partial f_s}{\partial\boldsymbol{\sigma}}\cdot\boldsymbol{D}^e\frac{\partial f_s}{\partial\boldsymbol{\sigma}} \quad (6)\sim(7)$$

in which, $\dot{\boldsymbol{\varepsilon}}$ is the strain increment tensor, $\dot{\boldsymbol{\sigma}}'$ is the effective stress increment tensor and the superscripts of e and $p$ denote the elastic and plastic components, respectively. Therefore, the stress and strain expression of the Sekiguchi and Ohta's model with the subloading surface is obtained as,

$$\dot{\boldsymbol{\sigma}}'=\left[\boldsymbol{D}^e-\frac{\left(K\beta\mathbf{1}+3G\frac{\boldsymbol{\eta}-\boldsymbol{\eta}_0}{\eta^*}\right)\otimes\left(K\beta\mathbf{1}+3G\frac{\boldsymbol{\eta}-\boldsymbol{\eta}_0}{\eta^*}\right)}{\beta^2K+2G+\frac{p'}{D}\left(\beta-mM\frac{\ln R}{R}\sqrt{\frac{\beta^2}{3}+\frac{3}{2}}\right)}\right]\dot{\boldsymbol{\varepsilon}}$$

$$\beta=M-\frac{3}{2\eta^*}\boldsymbol{\eta}\cdot(\boldsymbol{\eta}-\boldsymbol{\eta}_0) \quad (8)$$

in which $\boldsymbol{D}^e$ is 4th order elastic stiffness tensor, $\mathbf{1}$ is the unit tensor, $\boldsymbol{\eta}$ is the deviatoric stress ratio tensor ($\boldsymbol{\eta}=\frac{\boldsymbol{s}}{p'}$), $\beta$ is the accessibility function to the critical state, K is the elastic bulk modulus ($K=\frac{1+e_0}{k}p'$), $G$ is the elastic shear modulus ($G=\frac{3(1-2\nu)}{2(1+\nu)}K$, $\nu$: Poisson ratio) and $\otimes$ denotes the operator of tensor multiplier. The loading ($\dot{\boldsymbol{\varepsilon}}^p\neq\mathbf{0}$) or unloading ($\dot{\boldsymbol{\varepsilon}}^p=\mathbf{0}$) can be judged by the plasticity multiplier as,

$$\begin{cases}\Lambda<0: \text{unloading}\\ \Lambda=0: \text{neutral}\\ \Lambda>0: \text{loading}\end{cases} \quad (9)$$

Thus the obtained stress and strain relation is installed for input parameters of the finite element code, DACSAR (Iizuka and Ohta, 1987).

## Calibration of the Modeling

In this section, the simulation of shear behavior obtained from SBT under the condition of constant volume is presented. First of all, the input parameters are determined from the compression shear test results for disturbed sample (Fig. 1 (a) and (b)). The stress ratio, $(\tau/\sigma'_v)_f$ at the critical state in case of the direct shearing such as the shear box test under the condition of constant volume, can be derived by simultaneously solving the

critical state condition, and the undrained (constant volume) condition, $\dot{\epsilon}_v(=\dot{\epsilon}_v^e-\dot{\epsilon}_v^p)=0$ of Sekiguchi and Ohta's model, as (Ohta et al., 1993 ; Morikawa et al., 1997),

$$\left(\frac{\tau}{\sigma'_v}\right)_f=\frac{1+2K_0}{3\sqrt{3}}M \qquad (10)$$

With empirical relation of $K_0=1-\sin\phi'$ (Jaky, 1944), the critical state parameter, $M$ can be expressed by $(\tau/\sigma'_v)_f$ at $M=\frac{6\sin\phi'}{3-\sin\phi'}$. Here, the experimental value of $(\tau/\sigma'_v)_f$ is given in shear characteristics, though a little difference is found in the critical state lines with the water content. Herein, the kink point of effective stress path is chosen as the critical state point and then the critical state parameter, $M$ is determined to be 1.42. The compression index, $\lambda(=0.434C_c)$ can be directly determined to be 0.12 from compression characteristics of disturbed samples, because it is known that the gradient of compression line from $K_0$ consolidation in the $e-\ln\sigma_v'$ relation and that from the isotropic consolidation in the $e-\ln p'$ relation coincide with each other (Mitachi and Kitago, 1976). And the swelling index, $k$ is estimated as 0.023 from the empirical relation of $M=1.75(1-k/\lambda)$ (Karube, 1975), since the swelling index required as an input parameter in the constitutive model is the gradient of the isotropic swelling line. But, here, it differs from that of $K_0$ swelling line shown in Fig. 2 (a). The equivalent preconsolidation vertical stresses are determined from Fig. 7 with each water content. The lateral axis of effective normal stress is rewritten with a logarithm scale and $K_0$ swelling data in Fig. 2 (a) are plotted in Fig. 18, together with the compression lines.

The value of equivalent preconsolidation vertical stress is given as each intersection of Ko swelling line and the compression line with each water content value. The equivalent OCR is calculated as $\sigma'_{v0}/\sigma'_{vi}$ from the equivalent preconsolidation vertical stress and the current effective vertical stress. The coefficient of the current earth pressure at rest, $K_i$ is estimated from the empirical relation of $K_i=(OCR)^nK_0$ and n=0.42 (Ladd et al., 1977). Then, the assumed Poisson ratio, $\nu$ is 0.33.

The theoretical effective stress paths computed from the Sekiguchi and Ohta's model with the subloading surface using the above-determined input parameters are compared in Fig. 19 with the experimental results of shear characteristics of undisturbed samples, in which the parameters, $m$ defined in Eq.(4) are assumed to be 1.0 and 0.1. And the theoretical paths computed from the original Sekiguchi and Ohta's model without introducing the subloading surface are also compared. It cannot be said that the computed prediction well explains the shear behavior of compacted soil. But at least, it can successfully express the dilatancy characteristics of compacted soil and the case of *m=1.0* seems to give better prediction

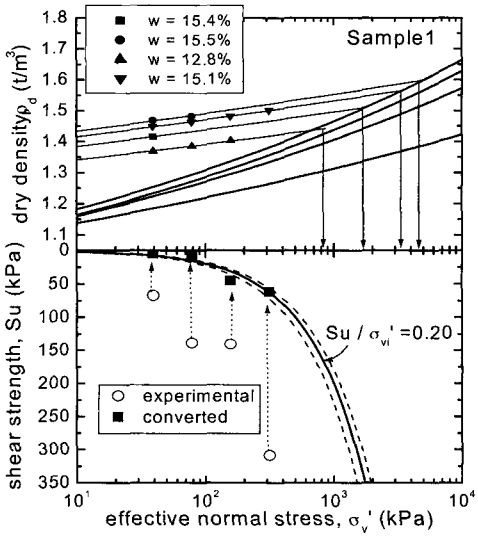


Fig. 18. Estimation of consolidation yield stress

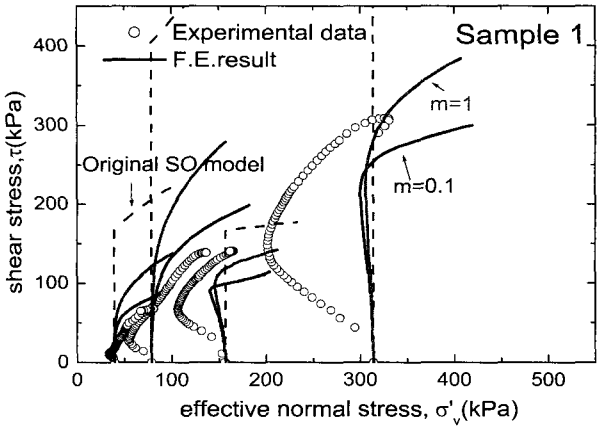


Fig. 19. Computed stress paths of compacted soil obtained from Sekiguchi and Ohta's model with the subloading surface and experimental data

for the compacted Omma sand.

### 3.2.2 The Result of Elasto-Plastic Finite Element Simulation

The material parameters needed in the elasto-plastic modeling of the compacted soil were already determined in the previous section. Now, it is necessary to estimate the equivalent preconsolidation vertical stresses in the compressive shear model tests. Figure 20 indicates the procedure to estimate the equivalent preconsolidation vertical stress considering the water content.

Since the evaluation of the initial effective vertical stresses in the specimen just before the compressive shear in the model test was very difficult, the equivalent preconsolidation vertical stress was determined as the value corresponding to the initial dry density of each specimen as shown in Fig. 18, which did not consider the slope of swelling line. Although the initial effective vertical stress, in reality, would be not uniform but is distributed in the specimen, the effective overburden pressure estimated at the center of specimen is employed in the computation as a representative value.

Figure 21 compares the computed load and displacement relation with the experimental results. In the figure, the black symbols, FEM 5 and FEM 9, denote the cases of well compacted specimen (high degree of compaction), corresponding to Test 5 and Test 9, respectively, while white symbols, FEM 6, FEM 7 and FEM 8, represent the cases of relatively poorly compacted specimen (relatively low degree of compaction), corresponding to Test 6, Test 7 and Test 8, respectively. Although the complete agreement between the computed and the measured results cannot be seen, it is found that the computed results, at least, explain the influence due to the difference of compaction degree. Moreover, it is found that introducing the subloading surface inside the normal yielding surface brings about smoother development of load and displacement curves, similar to the experimental results. Especially, the case of $m$=1.0, which controls the accessibility rate of the subloading surface to the normal yielding surface as defined in Eq.(4), seems to give better prediction.

Figures 22 and 23 compare the computed cross sectional area and circumference length of the specimen

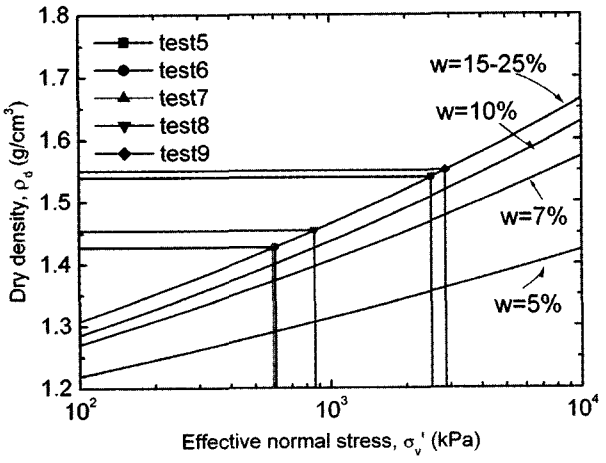


Fig. 20. Estimate of equivalent preconsolidation stress with water content

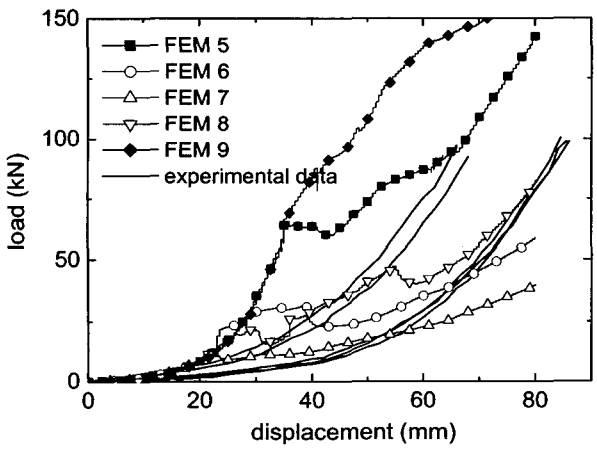


(a) Original Sekiguchi and Ohta's model

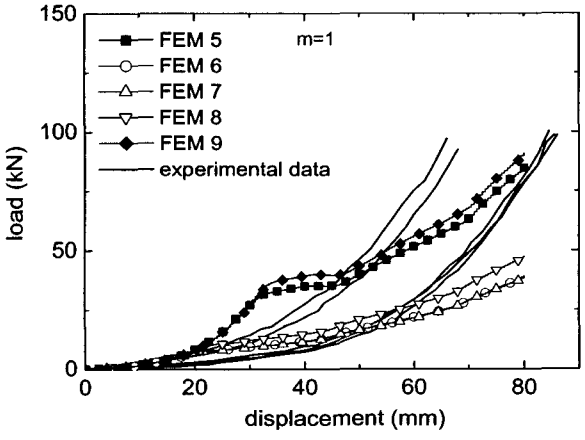


(b) Subloading model with m=1

Fig. 21. Computed load and displacement relation with experimental result

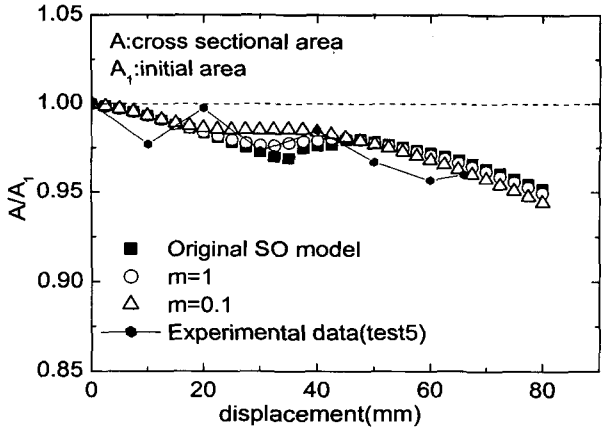


Fig. 22. Computed cross sectional area

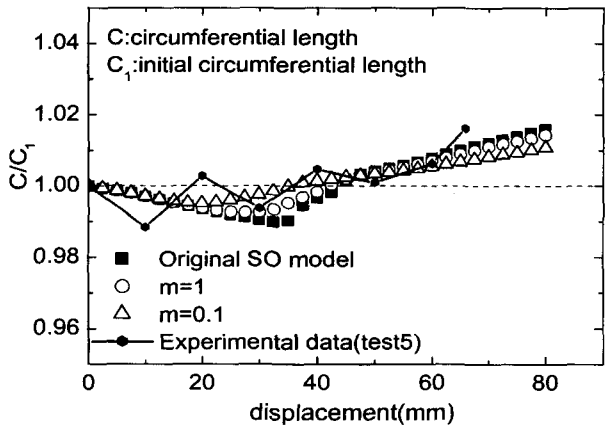


Fig. 23. Computed circumference length

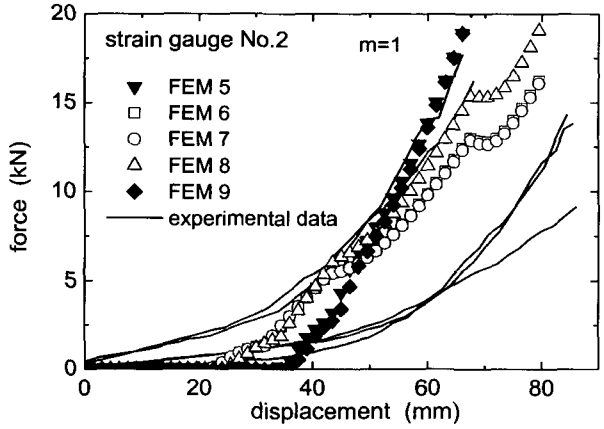


Fig. 24. Extension forces working on the geosynthetics with the displacement at the location for NO.2 strain gauge

with the measured results (test 5). It can be seen that the computed predictions well explain the measured results.

Figure 24 indicates the computed development of axial forces working on the geosynthetics with the displacement at the locations of the strain gauges No.2. The

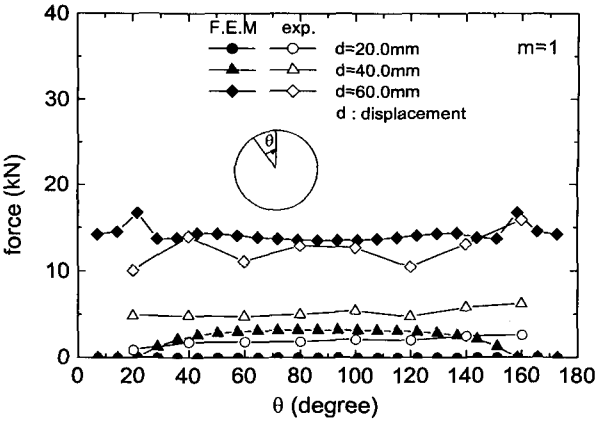


(a) well compacted specimen

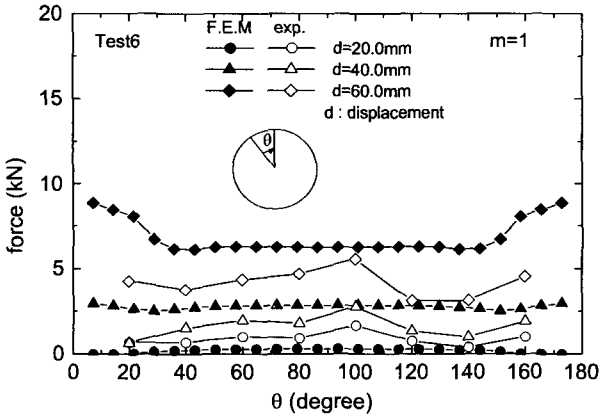


(b) relatively poorly compacted specimen

Fig. 25. Computed extension forces working to geosynthetics along circumference of specimen

calculated forces were compared with the measured results. And, Figure 25 show the computed distribution of axial forces along the circumference of the specimen, in which the case of high compaction degree (Test 5, FEM 5) is shown in Fig. 25 (a) and the case of relatively low compaction degree (Test 6, FEM 6) is in Fig. 25 (b). The elasto-plastic modeling with the subloading surface could well explain the measured results, in spite that the elastic modeling cannot explain the experiment as shown in Fig. 16.

## 4. Conclusion

This paper presents the methodology and the scheme to analyze the geosynthetic-reinforced soil structures and discusses the confining effect due to the geosynthetics wrapping the compacted soil specimen, and it

conducted a series of the compressive shear model tests and the finite element simulations. Particularly the mechanical interaction between the compacted soils and the geosynthetic-reinforcement materials are emphasized as a benchmark that should be taken into consideration in analyzing the geosynthetic-reinforcement effect.

A series of compressive shear tests for the compacted soil specimens wrapped by the geosynthetics are carried out and the geosynthetic-reinforcement effect is also examined. Here, as the initial degree of compaction is higher, the extension force gets higher with the displacement. Namely, the reinforcement effect by geosynthetics has close relation with the dilatancy characteristics of soils.

A series of elasto-plastic finite element simulations of the compressive shear tests are performed and the applicability of the simulation technique to the analysis of the geosynthetic-reinforcement mechanism is examined by comparing the computed prediction with the measured results. The elasto-plastic modeling with the subloading surface could well explain the measured results.

## References


1. Hashiguchi, K. (1989), "Subloading Surface Model in Unconventional Plasticity", *Int. J. of Solids and Structures*, Vol.25, pp. 917-945.
2. Iizuka, A., Ohta, H. (1987), "A Deformation Procedure of Input Parameters in Elasto-Viscoplastic Finite element analysis", *Soils and Foundations*, Vol.27, No.3, pp.71-87.
3. Iizuka, A., Hirata, M., Yokota, Y., Ohta, H., Kim, E.R., Kubo, T. (2002), "Compressive Shear Tests of Compacted Soils Wrapped by Geosynthetics", *Proc. of 7th International Conference on Geosynthetics*, IGS, Vol.3, pp.1133-1136.
4. Jaky, J. (1944), Tarajmechanika, *Journal of Hungarian Architecture and Engineering*, pp.355-358 (in Hungarian).
5. Jewell, R. A. (1991), "Application of revised design charts for steep reinforced slope", *Geotextiles and Geomembranes* 10, pp. 203-233 .
6. Karube, D. (1975), "Unstandardized Triaxial Testing Procedures and Related Subjects for Inquiry", *Proc. of 20th Symposium on Geotechnical Engineering*, pp.45-60 (in Japanese).
7. Ladd, C.C., Foott, R., Ishihara, K., Schlosser, F., Poulos, H.G. (1977), "Stress-Deformation and Strength Characteristics", *Proc. of 9th International Conference on Soil Mechanics and Foundation Engineering*, Vol.2, pp.421-494.
8. McGown, A., Andrawes, K. Z., and Al Hasani, M. M. (1978), "Effect of inclusion properties on the behavior of sand", *Geotechnique*, No.3, pp.161-166.
9. Mestat, P. (2001), MOMIS: A Database for the Numerical Modelling of Embankment on Soft Soils and the Comparison between Computational Results and In-situ Measurements, *Bulletin des Laboratories des Ponts et Chaussees*, Vol.232, Ref 4376, pp.45-60.
10. Mitachi, T., Kitago, S. (1976), "Change in Undrained Shear Strength Characteristics of Saturated Remolded Clay due to Swelling", *Soils and Foundations*, Vol.16, No.1, pp.45-58.
11. Morikawa, Y, Furuta, Y., Iizuka, A., Ohta, H. (1997), "Constant Volume Shear Strength of Clayey Soils", *Journal of Geotechnical Engineering*, JSCE, No.582/III-41, pp.173-182 (in Japanese).
12. Ohta, H. (1971), "Analysis of Deformation of Soils Based on the Theory of Plasticity and Its Application to Settlement of Embankments", *Thesis of Doctor of Engineering, Kyoto University.*
13. Ohta, H., Hata, S. (1977), "Strength of Dynamically Compacted Soils", *Proc. of 9th International Conference on Soil Mechanics and Foundation Engineering*, Tokyo, Vol.1, pp.239-242.
14. Ohta, H., Nishihara, A., Iizuka, A., Sugie, S. (1993), "Vane Strength in Anisotropically Consolidated Clay Deposits", *Journal of Geotechnical Engineering*, JSCE, No.481/III-25, pp.145-154 (in Japanese).
15. Sekiguchi, H., Ohta, H. (1977), "Induced Anisotropy and Time Dependency in Clays", Proc. Specialty Session 9, *9th International Conference on Soil Mechanics and Foundation Engineering*, Tokyo, pp.229-239.
16. Shibata, T. (1968), "On the Volume Change of Normally Consolidated Clays", *Technical Report of Disaster Prevention Research Institute*, Kyoto University, Vol.6, pp.128-134 (in Japanese).


(received on May 31, 2004, accepted on Jul. 5, 2004)